frontiers | Frontiers in Materials

TYPE Original Research
PUBLISHED 16 December 2022
DOI 10.3389/fmats.2022.1056620

OPEN ACCESS

EDITED BY
Cong Zhang,
Jiangnan University, China

REVIEWED BY
Jun He,
Changsha University of Science and Technology, China
Zhao-Dong Xu,
Southeast University, China

*CORRESPONDENCE
Zongping Chen,
zpchen@gxu.edu.cn

SPECIALTY SECTION
This article was submitted to Structural Materials,a section of the journal Frontiers in Materials

RECEIVED 29 September 2022
ACCEPTED 02 December 2022
PUBLISHED 16 December 2022

CITATION
Wang X, Li J, Huang L, Xie W and Chen Z (2022), Mechanical behavior of spiral reinforcement recycled aggregate concrete round columns under axial compression after spraying water at high temperatures.
Front. Mater. 9:1056620.
doi: 10.3389/fmats.2022.1056620

Mechanical behavior of spiral reinforcement recycled aggregate concrete round columns under axial compression after spraying water at high temperatures

Xin Wang[1], Junya Li[2,3], Leiqun Huang[4], Wangjun Xie[1] and Zongping Chen[2,3,5]*

[1]Guangxi Transport Vocational and Technical College, Nanning, China, [2]College of Architecture and Civil Engineering, Nanning University, Nanning, China, [3]College of Civil Engineering and Architecture, Guangxi University, Nanning, China, [4]Guangxi Road and Bridge Group Construction Engineering Co., Ltd., Nanning, China, [5]Key Laboratory of Disaster Prevention and Structure Safety of the Ministry of Education, Guangxi University, Nanning, China

Spiral hoops can effectively enhance the load-bearing capacity of recycled aggregate concrete columns, and the mechanical performance of such a member after experiencing fire and a fire sprinkler is very important for its application and promotion. Aiming at this problem, the mechanical behavior of spiral reinforcement recycled aggregate concrete round columns under axial compression after spraying water at high temperatures cooling was investigated. Three parameters including recycled coarse aggregate replacement ratio, temperature, and pitch of screw stirrups were taken into consideration. 26 specimens were designed for static loading test. The failure modes of regenerated concrete columns with spiral reinforcement were observed after cooling by high-temperature water spraying. The mechanical properties of specimens under different cooling modes after high temperatures were obtained and analyzed. The results indicate that the effect of the recycled aggregate replacement ratio on the performance of the specimens was mainly in terms of peak displacement. And the reduction in the spiral stirrup spacing increases the peak load and ductility coefficient of the specimens. The high temperature above 600°C has a obvious effect on the mechanical properties of the specimens. Water spray cooling can reduce the appearance of small cracks on the surface of the specimens and their peak displacement. The calculation method of bearing capacity of regenerated spiral reinforced concrete columns cooled by high-temperature water spraying was discussed.

KEYWORDS

spiral reinforcement recycled aggregate concrete, round columns, axial compression, spraying water at high temperature, mechanical behavior

1 Introduction

Recycled concrete refers to the new concrete prepared by mixing discarded concrete blocks with gradation in a certain proportion after processing, partially or fully replacing natural aggregates such as sand and gravel. The use of recycled aggregates, especially those from demolition waste or prefabricated concrete residues is an effective means of building green projects and maintaining sustainable development. (Behera et al., 2014). As an important part of recycled concrete application, reinforcement recycled concrete structure has the structural performance characteristics of reinforced concrete and the advantages of recycled coarse aggregate recycling. It has prominent application prospects in engineering practice. Researchers have not only conducted in-depth research on materials (Limbachiya et al., 2012.; Chen et al., 2014; Cao et al., 2016; Zheng et al., 2021)and components (Ajdukiewicz et al., 2007; Wang et al., 2011; Chen et al., 2013), but also carried out experimental research and theoretical analysis on the seismic performance of related specimens in terms of joints and structural systems. (Xiao et al., 2006; Cao et al., 2011; Liu et al., 2011; Lu et al., 2021; Xu et al., 2021).

In recent years, with the frequent occurrence of building fires, to provide the necessary basis for post-disaster safety assessment of structural components, it is particularly important to promote research on the residual bearing capacity of structural components after a fire disaster or high temperature. Researchers have also continued to advance their research on materials, computational methods and computational models. (Wu, 2003; Lu and Su, 2010; Ni and Gernay, 2020; Dai et al., 2021; Li et al., 2022; Yu et al., 2022; Shahraki et al., 2022; De Silva et al., 2022; Ge et al., 2022).

Currently, studies on the high-temperature resistance of recycled concrete structures are gradually gaining attention. Studies on the strength evolution, failure mechanism and residual strength of recycled concrete materials under the influence of high temperatures have shown that recycled aggregate concrete produced from recycled concrete, bricks and other construction wastes has a better quality performance at high temperatures (Garcia-Troncoso et al., 2013). The residual properties of them are similar to those of ordinary concrete (Laneyrie et al., 2016), but the strength degradation after high temperatures is greater than that of the ordinary one. With the growth of recycled aggregates' substitution rate, the rate of increase in the internal temperature of concrete and the fire resistance limit gradually decreases (Dong et al., 2013; Algourdin et al., 2022). The relative residual compressive strength of recycled concrete after high temperature will be greater than that of ordinary concrete under the same conditions when the substitution rate is greater than a certain threshold and is positively correlated with the substitution rate. (Xiao and Huang, 2006; Mohammad et al., 2021). Scholars have also studied the performance of steel-reinforced recycled concrete short columns, steel reinforced concrete T-shaped column,recycled concrete-filled steel tubes and cylinders after high temperatures, and explored the various factors affecting their performance (Chen et al., 2015; Wang et al., 2022; Chen et al., 2022).

The process of high temperature and rapid cooling would affect the development of micro-cracks and weaken the interface area, thus changing the physical and mechanical properties of concrete. (Ercolani et al., 2017). Different cooling methods can lead to differences in the mechanical properties of components that have experienced high temperatures. In practical engineering, most fires in buildings are extinguished by fire sprinklers. Studies have shown that spray cooling has a positive effect on the strength recovery of high-strength concrete after high temperatures (Chen et al., 2018).

With the characteristics of quick and convenient construction and molding of internally reinforced frames and good mechanical performance, spiral-reinforced restrained concrete columns have been widely used in practical engineering. The mechanical properties of recycled concrete reinforced with spiral reinforcement have been studied in depth in various aspects. (Woo et al., 2018; Muhammad J.M et al., 2019; Muhammad et al., 2020; Huang et al., 2021; Raza et al., 2021; Kumar et al., 2022). Spiral hoops can also play a positive role in improving the fire resistance of components (Zhou et al., 2022).

In the actual fire environment, buildings are often subjected to high temperatures along with the cooling effect caused by fire sprinkler cooling measures, which may have an impact on the mechanical property degradation pattern of recycled concrete. However, there is a lack of research on the performance of recycled concrete cylindrical members with spiral reinforcement after water spraying at high temperatures. Such a lack and ambiguity of assessment criteria threaten people's lives and can bring difficulties to post-disaster reconstruction and accountability, thus greatly limiting the further application of such structures.

To study the performance degradation law of spiral reinforcement recycled aggregate concrete round columns after high temperatures and spraying water cooling, three parameters including recycled coarse aggregate replacement ratio, temperature, and pitch of screw stirrups were taken into consideration as the variate. In this paper, each specimen's physical and mechanical properties are analyzed in depth through the comparison of axial compression tests. The formulae for calculating the residual bearing capacity are given to provide a reference for further research and post-disaster evaluation of spiral-reinforced recycled concrete cylindrical structures.

2 Experimental program

2.1 Preparation of specimens

A total of 26 recycled aggregate concrete cylindrical specimens with spiral stirrups were designed, and the section

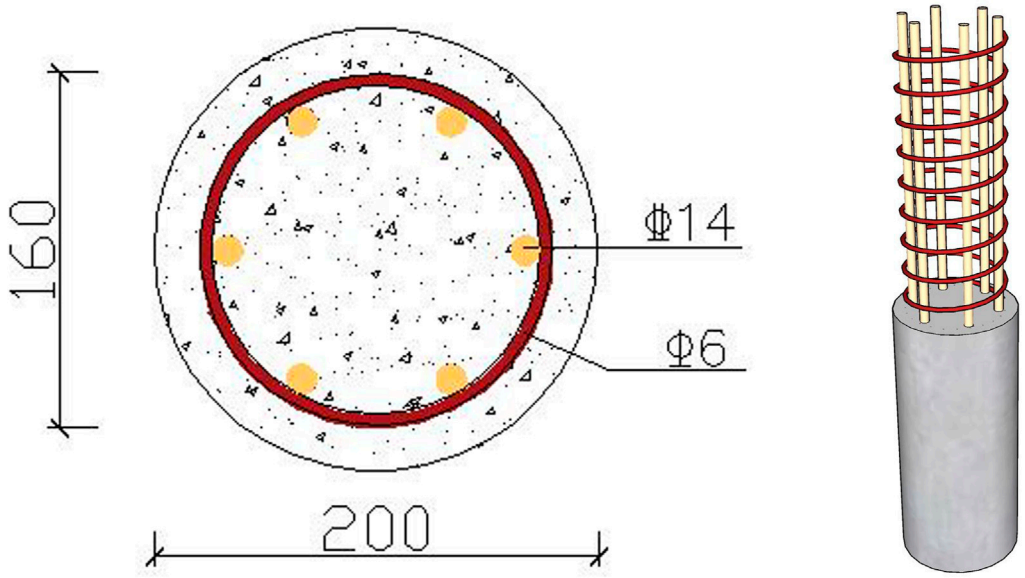

FIGURE 1
Cross-sectional dimensions and reinforcement.

size was uniform to a circular section of 200 mm in diameter. The height of the specimens was 910 mm, and the longitudinal reinforcement ratio was 2.94%. The Cross-sectional dimensions and reinforcement are shown in Figure 1.

Parameters such as the replacement rate of recycled coarse aggregate γ, temperature T, spiral stirrup spacing S, and cooling method after high temperature (natural cooling and spraying water cooling) were included in the design of the specimen considering. The specific design parameters are shown in Table.1.

2.2 Mechanical property of the material

The recycled coarse aggregate used in the specimens was obtained from the waste concrete test block with the original design strength of C30 in the laboratory, which was mechanically crushed and sieved. The size of recycled coarse aggregate is between 5 mm and 26.5 mm with continuous gradation. The natural coarse aggregates were also sieved under the same conditions. The physical property indexes of the coarse aggregates are shown in Table 2.

The specimens were made of ordinary river sand, ordinary Portland cement and urban tap water. and the mix proportion was designed according to the C30 strength standard. Recycled concrete is based on a replacement rate of 0%. Different replacement rates only change the proportion of recycled coarse aggregate and natural coarse aggregate. The specific mix ratio is shown in Table.3.

The HPB400 screw-thread steel bars with a diameter of 14 mm were used as the longitudinal reinforcement, and the HPB300 round bars with a diameter of 6 mm were used as the stirrup. According to the ***Metallic materials-Tensile testing-Part 1: Method of test at room temperature*** (GB/T 228.1-2010), the yield strength of the two kinds of two reinforcement are 442.32MPa and 439.77 MPa respectively, and the tensile ultimate strength is 570.44MPa and 618.24 MPa respectively. The international standard cylinder block with a size of 150 mm × 300 mm is reserved when the specimens were poured. The measured compressive strength fc is shown in Table.3.

2.3 Experimental equipment and cooling method

2.3.1 Heating equipment

The box-type industrial resistance furnace was used to raise the temperature of the test piece, The resistance furnace is 1200 mm × 600 mm × 400 mm in size, 45 kW in power and 950°C in rated temperature, and the heating equipment is shown in Figure 2A. The specimen was kept constant for 60 min in the furnace after reaching the target temperature, and the measured heating curve in the furnace is shown in Figure 2B. Due to the limitation of resistance furnace equipment, the temperature in the furnace will drop for a period during the heating process to 600°C and 800°C, then rise to the target temperature.

TABLE 1 Design parameters and burning loss rate.

Numbering	γ/%	T/°C	S/mm	Cooling method	Burning loss rate l/%
CRACC-1	0	20	30	—	—
CRACC-2	0	200	30	WC	.19
CRACC-3	0	400	30	WC	1.38
CRACC-4	0	600	30	WC	2.84
CRACC-5	0	800	30	WC	5.13
CRACC-6	30	600	30	WC	2.99
CRACC-7	30	800	30	WC	6.38
CRACC-8	50	600	30	WC	2.77
CRACC-9	50	800	30	WC	5.83
CRACC-10	70	600	30	WC	3.24
CRACC-11	70	800	30	WC	6.29
CRACC-12	100	20	30	—	—
CRACC-13	100	200	30	WC	0
CRACC-14	100	400	30	WC	.53
CRACC-15	100	600	30	WC	3.37
CRACC-16	100	600	50	WC	3.78
CRACC-17	100	600	70	WC	3.69
CRACC-18	100	800	30	WC	9.40
CRACC-19	100	800	50	WC	6.63
CRACC-20	100	800	70	WC	6.81
CRACC-21	100	600	30	NC	6.74
CRACC-22	100	600	50	NC	6.24
CRACC-23	100	600	70	NC	6.54
CRACC-24	100	800	30	NC	9.18
CRACC-25	100	800	50	NC	8.59
CRACC-26	100	800	70	NC	8.92

Note: γ is the replacement rate of recycled coarse aggregate; T is the maximum temperature experienced; S is the spacing of spiral stirrups; WC means water spraying cooling; and NC means natural cooling.

TABLE 2 Parameters of coarse aggregate.

The type of coarse aggregate	ρ_1/(kg/m^3)	ρ_0/(kg/m^3)	w/%	G_e/%
Natural coarse aggregate	1577	2701	0.70	12.4
Recycled coarse aggregate	1432	2639	3.79	14.0

Note: ρ1 is stacking mass density; ρ0 is the apparent mass density; w is water absorption and the Ge is the crushing index.

2.3.2 Cooling method

Based on the current actual firefighting situation, two cooling methods, natural cooling and spraying water cooling, were decided as the research arguments for the experiment. The specimens were first brought up to the target temperature and kept constant in the furnace for 60 min. Then the specimens were immediately removed and subjected to simulated fire sprinkler cooling. The specimen

TABLE 3 Concrete proportion.

γ/%	W/C	ρ	Material usage/(kg/m3)					Strength grade	f_c/MPa
			m_c	m_w	m_s	m_{NAC}	mRAC		
0	.43	.32	488.4	210	536	1139	0	C30	24.66
30	.43	.32	488.4	210	536	797.3	341.7		25.35
50	.43	.32	488.4	210	536	569.5	569.5		29.13
70	.43	.32	488.4	210	536	341.7	797.3		23.66
100	.43	.32	488.4	210	536	0	1139		25.42

Note: W/C is water-cement ratio; ρ is sand ratio; mc, mw, ms, mNAC, and mRAC are the dosages of cement, water, sand, natural coarse aggregate and recycled coarse aggregate, respectively.

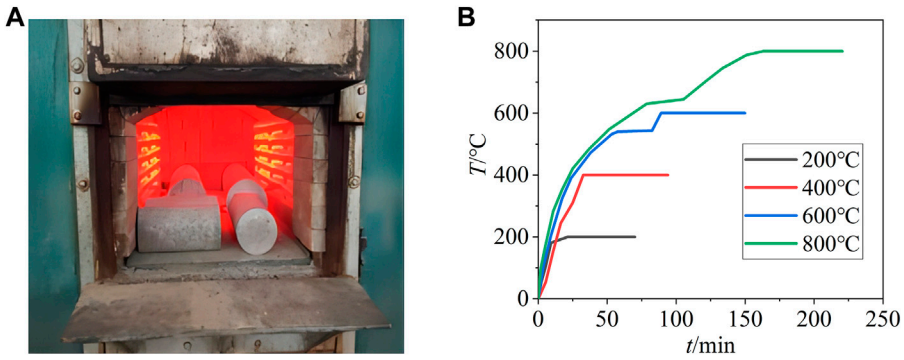

FIGURE 2
(A) Heating equipment **(B)** Furnace heating curves.

was continuously sprayed for 25 min, and the water flow shall be kept as consistent as possible. The specimens naturally cooled were kept in the resistance furnace until they were cooled to room temperature. The spray cooling in the test is shown in Figure 3.

2.3.3 Loading setup

The YAW-10000J microcomputer-controlled electro-hydraulic servo compression-shear test machine in the structural hall of Guangxi University was used to carry out the axial compression loading test of the specimens after high temperatures and spraying water cooling. Leveling should be done with a horizontal ruler before loading, and the uneven place was paved with fine sand. Both ends of the test piece were wrapped with FRP carbon fiber cloth and sleeved with specially processed hoops with a height of 5 mm to prevent the end from being damaged in advance. The displacement-controlled loading method was adopted in the test, and the loading rate was 1 mm/min. Stop loading when the load decreased by more than 85% or displacement deformation was over large. The loading setup is shown in Figure 4.

FIGURE 3
Water cooling.

FIGURE 4
Loading setup.

3 Experimental results and analysis

3.1 Change in the appearance

When the high temperature was completed, there was no obvious change in the surface of the specimens at 200°C and 400°C. There were a large number of irregular cracks on the surface of the specimens at 600°C and 800°C. At 800°C, the cracks were and the width was slightly larger than that at 600°C.

After spraying water cooling, there was no obvious phenomenon in the specimen at 200°C, weak white smoke was generated in the specimen at 400°C, and there was no obvious change in the appearance of the specimen after spraying water at 200°C and 400°C. At 600°C, the specimen produced white smoke under the action of water spraying. After water spraying, the fine cracks on the surface of the specimen were weakened and reduced, and there was a small amount of loss on the surface. At 800°C, the specimen produced a large amount of white smoke under the action of water spraying. After it, there is still few white smokes produced. The fine cracks on the surface were also weakened and reduced, water stains appeared at the cracks, and the surface loss was relatively serious.

After spray cooling, at 200°C, the specimen had no obvious change compared with normal temperature. At 400°C, the color of the specimen slightly deepened, showing light gray and yellowish. When the temperature reached 600°C, the surface color of the specimen became deeper and yellowish, and many irregular cracks appear. At 800°C, the specimen surface turned grayish-white, and there were more irregular cracks on the surface. Apparent changes in specimens before and after spraying is shown in Figure 5.

3.2 High temperature burning loss rate of specimens

The specimens under different cooling methods before and after high temperatures were weighed to obtain the mass loss rate after high temperatures. Figure 6A shows the relationship between the temperature and burning loss rate of each specimen after high-temperature water spraying under different recycled coarse aggregate replacement rates. Among the picture, WC means water spraying cooling, and NC means natural cooling.

It can be seen from the figure that with the increase in temperature, the burning loss rate of the specimen increases gradually. The mass of the specimen is almost not lost at 200°C. At 400°C, the burning loss rate of the specimen increases slightly, but it is not obvious for the whole. At 600°C, there is little difference in the loss on ignition rate of each substitution rate. At 800°C, the specimen concrete becomes crisp, the surface appears peeling phenomenon, and the burning loss rate is relatively large.

Figure 6B shows the relationship between the burning loss rate and temperature of specimens with different spacing spiral stirrups under different cooling methods. It can be seen from the figure that the overall burning loss rate under natural cooling is higher than that under spray cooling, and the effect of spiral stirrup spacing on the burning loss rate is not obvious. This is because the quality loss of the naturally cooled specimens is mainly due to the evaporation of water

FIGURE 5
Apparent changes of specimens after spraying.

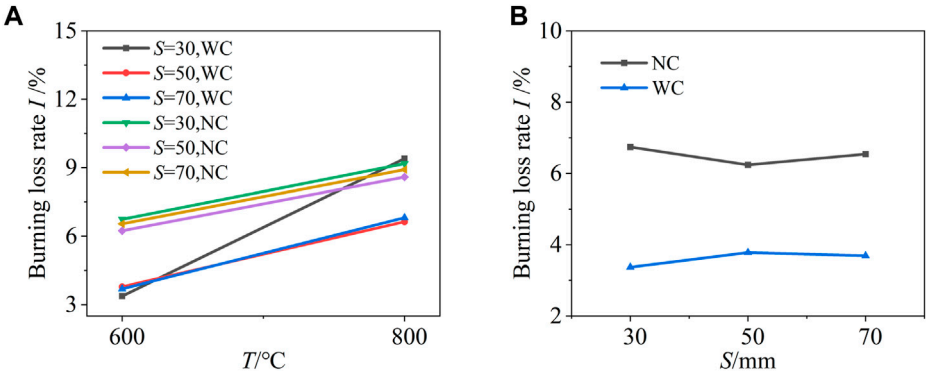

FIGURE 6
Influence of different factors on burning loss rate. **(A)** Coarse aggregate replacement ratio; **(B)** Cooling method and stirrup spacing.

and the peeling and flaking of the concrete; while the specimens cooled by water spraying, although a large amount of water evaporated during the process of exposure to high temperature, in the process of simulated fire spraying, some of the water re-infiltrated into the interior of the specimens and a series of chemical reactions occurred with the aggregates, and the quality of the specimens increased during this process compared to the effect of high temperature.

3.3 Failure process and shape of the specimen under stress

The overall failure process of spiral-reinforced concrete specimens was roughly the same. After the vertical cracks appeared, the outer concrete peeled off, the inner core concrete continued to maintain the bearing capacity for a while, and the final specimens were damaged due to excessive deformation or stirrups crushed by longitudinal reinforcement.

At room temperature and 200°C, the first vertical crack appeared at about 0.8 N_u (N_u is the peak load). With the increase in load, the inclined crack zone was formed on the surface of the specimen, and the concrete protective layer was massively exfoliated. Due to the confinement effect of stirrups, the specimen continued to be subjected to force for a while, and then the longitudinal reinforcement of the specimen was deformed too large to squeeze out the spiral reinforcement, and the specimen was destroyed. At 400°C, the first vertical crack appeared around 0.7 N_u, and with the increase of load, multiple parallel vertical cracks were formed in the outer concrete. At 600°C, vertical

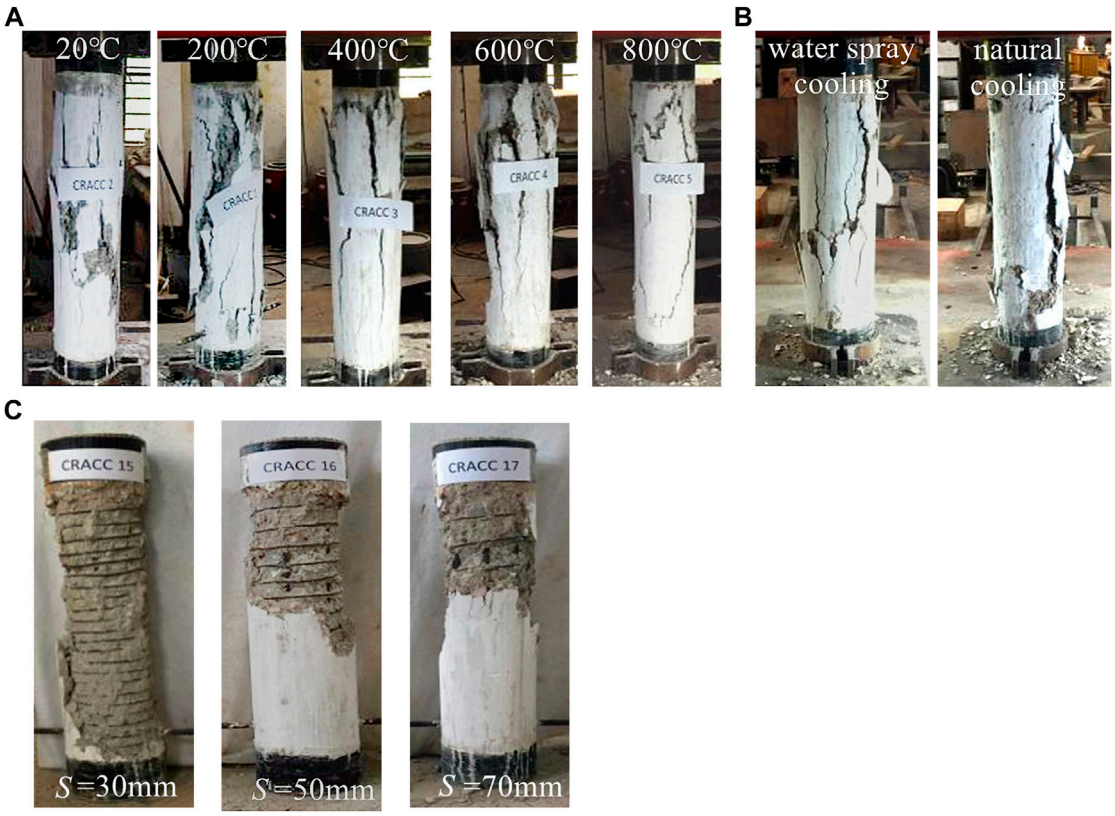

FIGURE 7
Final failure modes. **(A)** Failure modes of specimens at different temperatures; **(B)** Failure modes of specimens under different cooling methods; **(C)** Failure modes of specimens with different spiral reinforcement space.

cracks appeared in the specimen at about 0.5–0.6 N_u. The cracks developed irregularly with the increase in load, and then the concrete peeled off. At 800°C, vertical cracks appeared in the specimen about 0.3–0.4 N_u, the load increased gradually, and the spalling volume of concrete was also larger. The failure process under different temperatures is shown in Figure 7A.

Figure 7B shows the failure modes under different cooling methods. Compared with the specimens cooled by spraying, the cracks appeared relatively later and the stripped volume of concrete was smaller in the specimens under natural cooling.Figure 7C shows the failure modes under different spiral reinforcement spacing. The concrete spalling volume tends to be positively correlated with the spiral reinforcement spacing.

3.4 Main parameters of feature points

The main parameters of specimens under different cooling methods after high temperature, including peak load N_u, peak displacement Δp, initial stiffness EA and displacement ductility coefficient μ are given in Table. 4. The initial stiffness EA takes the secant stiffness of .4 times the peak load point at the rising section of the load-displacement curve. In displacement ductility coefficient $\mu = \Delta u/\Delta y$, Δu takes the corresponding displacement when the load drops to 85% peak load, and Δy is the yield displacement value, which is determined by referring to the general yield bending moment method.

3.5 Load-displacement curves

The axial load-displacement curve of the specimen during the whole failure process was obtained, as shown in Figure 8. Among them, γ is the recycled coarse aggregate replacement ratio, S is the spacing of spiral stirrups; WC means spraying water cooling, and NC means natural cooling. The figure shows that the peak load of the specimen will decrease with the increase in temperature. Peak displacement fluctuates within a certain range at 600°C and lower temperatures, but the difference is not significant.

However, at 800°C, the peak displacement of the specimen will increase significantly. The higher the temperature is, the

TABLE 4 Main parameters of feature points.

Numbering	γ/%	T/°C	Cooling method	N_u/kN	Δ_p/mm	EA/MN	Δ_y/mm	Δ_u/mm	μ
CRACC-1	0	20	—	1376.0	13.846	253.859	6.415	25.047	3.90
CRACC-2	0	200	WC	1295.0	11.579	256.033	5.697	26.700	4.69
CRACC-3	0	400	WC	1256.5	10.937	199.248	7.699	22.195	2.88
CRACC-4	0	600	WC	1265.0	11.807	183.962	8.847	24.959	2.82
CRACC-5	0	800	WC	1168.5	18.034	134.225	10.050	24.020	2.39
CRACC-6	30	600	WC	1311.0	12.656	167.012	9.489	26.327	2.77
CRACC-7	30	800	WC	1133.0	20.185	112.861	11.795	30.447	2.58
CRACC-8	50	600	WC	1443.5	8.843	241.113	6.972	13.328	1.91
CRACC-9	50	800	WC	942.0	17.320	159.602	7.242	>21.749	>3.00
CRACC-10	70	600	WC	1373.0	11.916	270.391	8.116	23.663	2.92
CRACC-11	70	800	WC	1184.0	17.224	148.589	10.343	26.283	2.54
CRACC-12	100	20	—	1326.5	12.863	261.308	5.809	>28.128	>4.84
CRACC-13	100	200	WC	999.5	8.710	214.630	5.577	22.195	3.98
CRACC-14	100	400	WC	1226.0	19.707	187.596	8.987	>27.671	>3.08
CRACC-15	100	600	WC	1319.0	13.801	186.704	9.043	22.496	2.49
CRACC-16	100	600	WC	1137.0	7.751	224.777	5.725	11.266	1.97
CRACC-17	100	600	WC	1040.0	8.112	189.404	5.801	10.223	1.76
CRACC-18	100	800	WC	674.0	22.784	88.787	9.757	>34.074	>3.49
CRACC-19	100	800	WC	929.0	13.003	121.049	9.360	19.763	2.11
CRACC-20	100	800	WC	841.5	10.776	128.670	7.695	15.514	2.02
CRACC-21	100	600	NC	1017.5	12.851	177.652	6.909	29.115	4.21
CRACC-22	100	600	NC	1160.5	8.903	229.683	5.822	11.430	1.96
CRACC-23	100	600	NC	1045.5	6.792	243.448	4.802	9.344	1.95
CRACC-24	100	800	NC	793.5	20.301	120.960	8.818	31.226	3.54
CRACC-25	100	800	NC	713.0	10.087	104.853	7.735	18.688	2.42
CRACC-26	100	800	NC	564.0	9.472	400.624	6.191	14.255	2.30

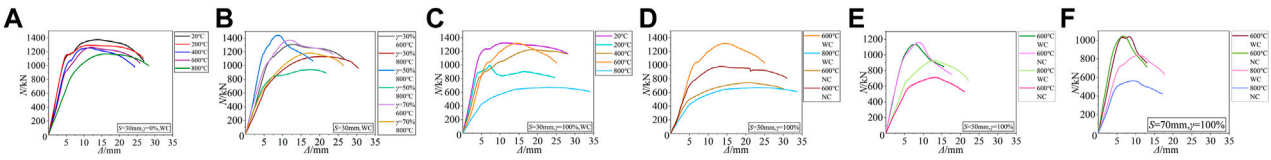

FIGURE 8
Load-displacement curves. **(A)** S = 30 mm, γ = 0%, WC; **(B)** S = 30 mm, WC; **(C)** S = 30 mm, γ = 100%, WC; **(D)** S = 30 mm, γ = 100%; **(E)** S = 50 mm, γ = 100%; **(F)** S = 70 mm, γ = 100%.

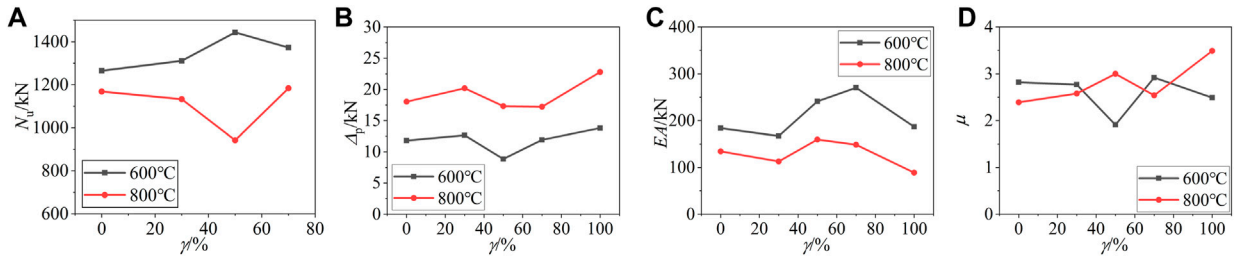

FIGURE 9
Influence of replacement ratio on mechanical properties. **(A)** peak load; **(B)** peak displacement **(C)** initial stiffness **(D)** displacement ductility coefficient.

smaller the initial secant slope of the curve is, and it decreases significantly after 600°C, the initial secant slope after high temperatures and spraying water cooling is higher than that after natural cooling, which is more obvious at 800°C.

4 Analysis of influencing factors

4.1 Replacement ratio of recycled coarse aggregate

According to Table.4, when the maximum temperature is less than 400°C, the peak load of the specimen decreases slightly with the increase of the replacement ratio. Compared with the 0% replacement ratio specimen, the 100% replacement rate specimen decreases by 3.6% and 2.4% respectively at room temperature and 400°C. Figure 9A shows the curve of peak load *versus* replacement ratio at high temperatures. When the maximum temperature is 600°C, the peak load of specimens increases slightly with the increase in replacement ratio, and the peak load of specimens with 30%–70% replacement rates increases by 3.6%,1.4%, and 8.5%, respectively. When the maximum temperature reaches 800°C, the peak load of the specimen fluctuates with the increase of the substitution rate, but the overall trend is still slightly upward. Overall, the replacement rate of recycled aggregate has little effect on the peak load of the specimen.

The peak displacement of fully recycled concrete specimens is lower than that of ordinary concrete specimens at room temperature and 200°C, 15.6%, and 33.0% respectively. Figure 9B shows the graph curves of the peak displacement of the specimen with the replacement rate at high temperatures. The peak displacement of specimens with the highest temperature of 600°C or 800°C increases with the increase in replacement rate. And the rise in peak displacement is greater for specimens experiencing a temperature of 800°C.The peak displacement of specimens with 30%–100% replacement ratio increase by 3.0%, −20.4%, 3.2%, and 17.8% respectively at 600°C. At 800°C, it increases by 21.8%, 7.4%, 8.5%, and 36.2% respectively.

Figure 9C shows the curves of the initial stiffness of the specimen with the change of replacement ratio at different temperatures. It can be seen from the figure that when the maximum temperature is 600°C or 800°C, the initial stiffness decreases firstly and then recovers, and finally decreases again with the increase of the replacement ratio. On the one hand, compared with natural coarse aggregates, recycled coarse aggregates have higher water absorption, and the water content of recycled concrete is larger under the same environmental conditions. Under high-temperature conditions, the recycled concrete has more evaporable water, and to a certain extent, the evaporation of water can slow down the increase of internal temperature of concrete, thus reducing the damage of high temperature on the elastic modulus of concrete; on the other hand, due to the existence of physical defects such as micro-cracks at the interface between cement and recycled coarse aggregate, the recycled concrete itself has mechanical property defects, and the larger the replacement rate of recycled coarse aggregate. On the other hand, because of the physical defects such as micro-cracks at the interface between cement and recycled coarse aggregate, the recycled concrete itself has mechanical defects, and the larger the substitution rate of recycled coarse aggregate, the more serious the mechanical defects will be. When $\gamma < 30\%$ or $\gamma > 70\%$, the latter plays a dominant role, so with the increase of replacement rate, the modulus of elasticity of recycled concrete gradually decreases, and the axial compression stiffness of steel pipe recycled concrete specimens also gradually decreases; when $30\% < \gamma < 70\%$, the former plays a dominant role, the result is the opposite.

On the whole, the average ductility of specimens with a 100% substitution rate is 6.7% higher than that of specimens with a 0% substitution rate. Figure 9D shows the variation curve of the displacement ductility coefficient with replacement ratio. When the maximum temperature is 600°C or 800°C, the ductility of the specimen changes

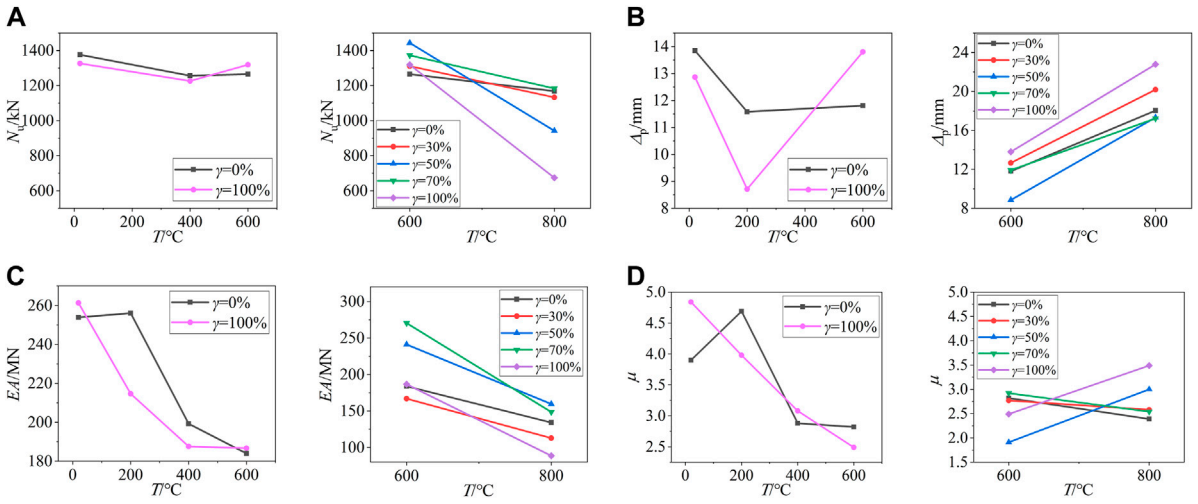

FIGURE 10
Influence of temperature on mechanical properties. **(A)** peak load; **(B)** peak displacement **(C)** initial stiffness **(D)** displacement ductility coefficient.

relatively small with the change of replacement ratio. At 800°C, with the increase of the replacement ratio, the ductility of the specimen will increase slightly.

4.2 Temperature

Figure 10A shows the variation curves of the peak load with temperature under different replacement rates. It can be seen from the figure that when the temperature is 400°C, the bearing capacity of the specimen will decrease slightly with the increase in temperature. This is because the free water inside the concrete is lost after the specimen experiences a high temperature of 400°C, and the concrete absorbs a large amount of free water when spraying water. The change of temperature difference in this process will cause the internal deformation of the concrete to be uncoordinated to a certain extent, resulting in micro-cracks, which will reduce the bearing capacity of the concrete; At 400°C–600°C, because of the uneven temperature field inside and outside the concrete during the heating process, the temperature rise process of the internal concrete will be relatively slow, and the existence of spiral stirrup will make this process slower. Therefore, the performance damage of internal core concrete can be alleviated to a certain extent by spraying water cooling immediately after high temperature. Consequently, the bearing capacity of specimens after high-temperature water spraying cooling is relatively flat. When the maximum temperature is between 600°C and 800°C, the core concrete is subjected to high temperatures. The loss of free water and bound water causes severe damage to its internal structure, which leads to a continued decrease in the bearing capacity of the specimen.

Figure 10B shows the curves of peak displacement *versus* temperature under different replacement ratios. It can be seen from the figure that the peak displacement of the specimen fluctuates in the range of 10 mm–14 mm when the temperature is less than 600°C. Among them, the peak displacement was slightly lower at 200°C. At 800°C, the peak displacement of the specimen was significantly increased. Compared with the specimen experiencing the highest temperature of 600°C, the peak displacement of the specimen experiencing the highest temperature of 800°C with different substitution rates increased by 38% on average. This may be caused by the evaporation of water inside the specimen after high temperature and becoming loose, and the concrete being continuously compacted before the peak load.

Figure 10C shows the variation curves of the initial stiffness of the specimen with temperature under different substitution rates. It can be seen from the figure that with the increase in temperature, the initial stiffness of the specimen generally shows a continuous downward trend. When the maximum temperature is below 600°C, the decrease in the initial stiffness of the specimen is relatively small. When the maximum temperature is 600°C, the initial stiffness of 0% and 100% specimens decreases by 27.53% and 28.6% respectively compared with the specimens at room temperature. When the temperature is between 600°C and 800°C, the initial stiffness decreases slightly, and the initial stiffness of the specimens with 0%–100% replacement ratio decreased by 27%, 32.4%, 33.8%, 45%, and 52.4%, respectively.

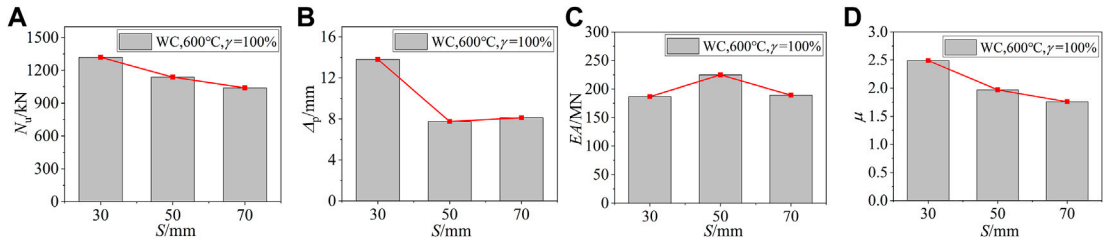

FIGURE 11
Influence of spacing on mechanical properties. **(A)** peak load; **(B)** peak displacement **(C)** initial stiffness **(D)** displacement ductility coefficient.

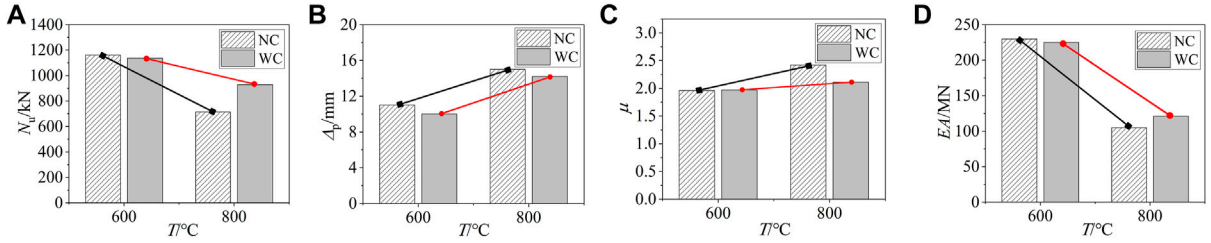

FIGURE 12
Influence of different cooling methods on mechanical properties. **(A)** peak load; **(B)** peak displacement **(C)** initial stiffness **(D)** displacement ductility coefficient.

Figure 10D shows the curves of displacement ductility *versus* temperature under different replacement ratios. It can be seen from the figure that the ductility of specimens with a 0% replacement rate and a 100% replacement rate decreases with the increase in temperature. When the maximum temperature was 600°C, the ductility of specimens with 0% and 100% replacement rates decreased by 27.7% and 48.6%, respectively. However, when the maximum temperature is between 600°C and 800°C, the ductility coefficient of the specimen is relatively stable, and the ductility of the specimens with different replacement rates is not much different at the same temperature.

4.3 Spiral stirrup spacing

The specimens with the highest temperature of 600°C, cooling by spraying and substitution rate of 100% were taken to study the influence of stirrup spacing on each performance. Figure 11 shows the variation curves of mechanical properties of specimens with the increase of stirrup spacing S. The peak load of specimens with 30mm, 50mm, and 70 mm spacing decreases nearly linearly. The peak load of specimens with 50mm and 70 mm spacing is 13.8% and 21.2% lower than that of specimens with 30 mm spacing. The peak displacement of specimens with 50 mm spacing is 37.9% lower than that of specimens with 30 mm spacing, while the peak displacement of specimens with 70 mm spacing is similar to that of specimens with 50 mm spacing, which is 36.5% lower than that of specimens with 30 mm spacing. The initial stiffness of the specimen with 50 mm spacing is the largest among the three specimens, which increases by 20.4% compared with the specimen with 30 mm spacing, while the initial stiffness of the specimen with 70 mm spacing is similar to that of the specimen with 30 mm spacing, which increases by 1.4%. The ductility coefficient decreases with the increase of stirrup spacing. Compared with 30 mm spacing specimens, 50mm and 70 mm spacing specimens decrease by 20.9% and 29.3% respectively. This is because the spiral reinforcement produces a larger restraint on the specimen, the smaller the hoop spacing, the more obvious the restraint effect, so the better the ductility of the specimen and the more fully the reinforcement plays its role.

4.4 Cooling method

Figure 12 shows the difference in mechanical properties of the recycled concrete cylinder with spiral reinforcement under different cooling methods. It can be seen from the figure that

there is little difference in the peak load between the two cooling methods at 600°C. At 800°C, the peak load of the natural cooling specimen decreases more than that of the spraying water cooling specimen, and the peak load decreases by 23.3% compared with the specimens cooled by spraying water. This may be because when the specimen experiences a temperature of 800°C, its internal water evaporates a lot, and in the process of water spraying cooling, the water penetrates the interior of the specimen under the action of water pressure and a series of physical or chemical reactions occur with the aggregate, thus strengthening the bearing capacity of the specimen.

The peak displacement of specimens under natural cooling is always larger than that under spray cooling, which is 10% and 5% higher at 600°C and 800°C, respectively. Different cooling methods have no significant effect on the initial stiffness of the specimen. At 600°C, the ductility coefficient of the specimen after water spraying cooling and natural cooling has little difference. At 800°C, the ductility coefficient after natural cooling is greatly improved than that after water spraying cooling. This is since compared to natural cooling, at the same temperature, spraying water cooling causes a drastic temperature change, which produces more serious damage to the concrete in a short period, making the cracks at the interface between cement and recycled coarse aggregate larger, and therefore the greater the defect in the mechanical properties of concrete.

5 Bearing capacity analysis

5.1 Damage analysis

Recycled concrete with spiral reinforcement is subject to considerable damage after the action of high temperatures, resulting in a reduction of the structural load-bearing capacity. According to the damage theory, the high temperature leads to defects in the specimen, reducing the effective section. Therefore, the parameter D is introduced to describe the damage degree of the specimen.

$$D = 1 - \frac{S^*}{S}. \tag{1}$$

In Eq. 1, S and S^* denote respectively the sum of the cross-sectional area under non-destructive conditions and the effective area after damage.

Since the resultant force of specimens before and after the damage is equal, Eq. 2 can be obtained:

$$\sigma \cdot S = \sigma^* \cdot S^*. \tag{2}$$

According to the hypothesis of equivalent strain, Eq. 3 is obtained as follows. σ and σ^* are the effective stress before and after damage, respectively. E and E^* indicate the modulus of elasticity when the material is undamaged and the modulus of elasticity after damage, respectively. ε is the stress caused by the effective stress acting on the damaged material or the stress caused by it under non-destructive conditions.

$$\varepsilon = \frac{\sigma^*}{E} = \frac{\sigma}{E^*}. \tag{3}$$

According to the above formula, Eq. 4 can be derived as follow:

$$\sigma = E\varepsilon(1 - D). \tag{4}$$

Considering the initial defects caused by high-temperature damage on the specimen, to define the damage degree of high-temperature specimens (200°C, 400°C, 600°C, and , 800°C), the elastic modulus E of the specimen at room temperature (20°C) is used to determine the elastic modulus E_0 at non-destructive (Su, Z. and Chen, Z., 2021; Sun, B., et al., 2022), and Eq. 5 can be obtained:

$$D = 1 - \frac{E_T}{E_0}. \tag{5}$$

In Eq. 5, E_T is the elastic modulus of the specimen cooled by spraying after high temperature: E_0 is the elastic modulus of specimens at room temperature. The larger the D value, the greater the damage to the specimen.

Figure 13A shows the variation trend of the damage degree with temperature under different substitution rates. It can be seen that the higher the temperature of the specimen is, the greater the damage degree is. When the temperature is less than 600°C, the damage degree of the specimen rises little with the increase in temperature, but when the temperature reaches 800°C, the damage degree of the specimen increases sharply. The addition of recycled coarse aggregate will increase the damage to the concrete after high temperatures and spraying water cooling. Compared with ordinary spiral-reinforced concrete, the damage degree of spiral-reinforced recycled concrete block is more severely affected by temperature.

The specimens with the maximum temperature of 600°C and the replacement rate of the recycled coarse aggregate of 800°C were taken to study the influence of spiral reinforcement spacing and cooling method on the damage degree. As shown in Figure 13B, when the spray cooling method is adopted, the D decreases first and then increases with the increase of spacing. The damage is minimized when the spacing is 50 mm. When natural cooling is adopted, the D decreases with the increase of spacing. When the spacing of spiral reinforcement is 30 mm, the damage of the specimen can be reduced by spray cooling, but when the spacing is 50 mm and 70 mm, the damage of the specimen increases.

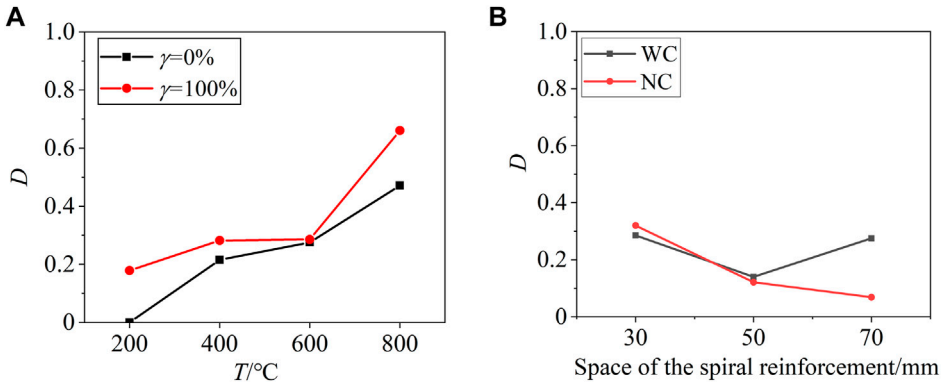

FIGURE 13
(A) The change of damage degree of specimens with temperature under different substitution rates. **(B)** Effect of spiral rib spacing on damage degree under different cooling methods.

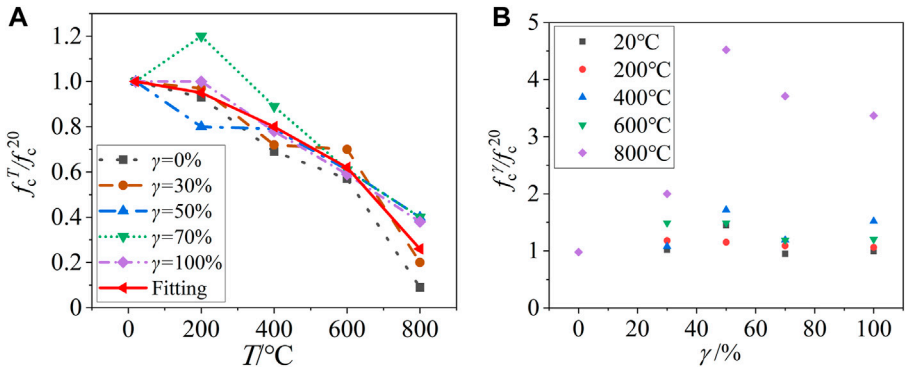

FIGURE 14
(A) Effect of temperature on strength of specimen; **(B)** Effect of replacement ratio on strength of specimens.

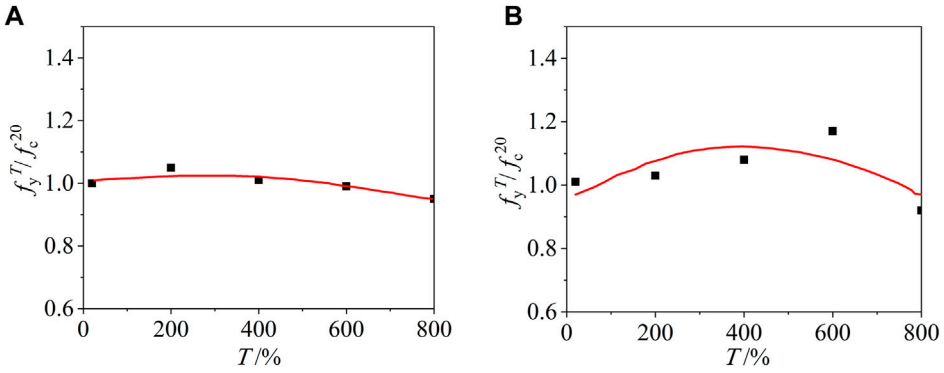

FIGURE 15
Effect of temperature on tensile strength of reinforcement. **(A)** longitudinal reinforcement; **(B)** stirrup.

TABLE 5 Comparison between calculated and measured values of bearing capacity of specimens.

Numbering	γ/%	T/°C	Cooling method	Bearing capacity/kN		Calculated value/Test value
				Calculated value	Test value	
CRACC-1	0	20	WC	1128.6	1376	.82
CRACC-2	0	200	WC	1173.4	1295	.91
CRACC-3	0	400	WC	1137	1256.5	.90
CRACC-4	0	600	WC	1057.4	1265	.84
CRACC-5	0	800	WC	860.4	1168.5	.74
CRACC-6	30	600	WC	1061	1311	.81
CRACC-7	30	800	WC	1030.1	1133	.91
CRACC-8	50	600	WC	1063.4	1443.5	.74
CRACC-9	50	800	WC	1093.3	942	1.16
CRACC-10	70	600	WC	1065.9	1373	.78
CRACC-11	70	800	WC	1116.5	1184	.94
CRACC-12	100	20	WC	1129.6	1326.5	.85
CRACC-13	100	200	WC	1192.3	999.5	1.19
CRACC-14	100	400	WC	1152.5	1226	.94
CRACC-15	100	600	WC	1069.5	1319	.81
CRACC-16	100	600	WC	890.1	1137	.78
CRACC-17	100	600	WC	813.2	1040	.78
CRACC-18	100	800	WC	1076.4	674	1.60
CRACC-19	100	800	WC	917.1	929	.99
CRACC-20	100	800	WC	848.8	841.5	1.01
CRACC-21	100	600	NC	1069.5	1017.5	1.05
CRACC-22	100	600	NC	890.1	1160.5	.77
CRACC-23	100	600	NC	813.2	1045.5	.78
CRACC-24	100	800	NC	1076.4	793.5	1.36
CRACC-25	100	800	NC	917.1	713	1.29
CRACC-26	100	800	NC	848.8	564	1.50

5.2 Bearing capacity analysis

The performances of recycled concrete and steel bars are quite different after spraying water at high temperatures. The bearing capacity of reinforced recycled concrete members composed of the two is also quite different from that of members without spraying water at high temperatures. Therefore, the use of the conventional formula for calculating the residual bearing capacity of spiral-reinforced recycled concrete will lead to a significant difference between the calculated value and the actual situation. It is necessary to modify the coefficient of the existing bearing capacity formula of spiral stirrup members in the specification.

According to the influence of temperature and recycled coarse aggregate replacement rate on the strength of recycled concrete cylinder blocks, the data were normalized and fitted to obtain the influence law of temperature and replacement rate on the strength of recycled concrete. Depending on the significant difference in the rate of decrease in strength of specimens at different temperature stages, the curves were divided into three different temperature segments: $20^{\circ}C \leq T < 200^{\circ}C$, $200^{\circ}C \leq T \leq 600^{\circ}C$, $600^{\circ}C < T \leq 800^{\circ}C$ for regression fitting.

The effect of temperature on the strength of recycled concrete block is obtained by the above method as shown in Figure 14A. (f_c^T represents the strength of the material after experiencing different temperatures, f_c^{20} represents the strength of the material at room temperature, and f_c^{γ} represents the compressive strength at different substitution rates)

$$N = \alpha_1 \beta f_c A_{cor} + \alpha_2 f_y A_s + 2\alpha_3 f_{yt} \frac{\pi d_{cor} A_{st}}{s}, \quad (6)$$

$$\alpha_1 = \begin{cases} -0.27 \times \dfrac{T}{800} + 1.007, & 0°C \le T \le 200°C \\ -0.68 \times \dfrac{T}{800} + 1.11, & 200°C \le T \le 600°C \\ -1.32 \times \dfrac{T}{800} + 1.59, & 600°C \le T \le 800°C \end{cases} \quad (7)$$

$$\alpha_2 = -3 \times 10^{-7} T^2 + 0.0002T + 1.0065 \; 20°C \le T \le 800°C, \quad (8)$$

$$\alpha_3 = -1 \times 10^{-6} T^2 + 0.0008T + 0.9522 \; 20°C \le T \le 800°C, \quad (9)$$

$$\beta = \begin{cases} 0.0031\gamma + 1.0384, & 0°C \le T \le 200°C, \\ 0.067\gamma + 1.0748, & 200°C \le T \le 600°C, \\ -6.175\gamma^2 + 8.8457\gamma + 0.7932, & 600°C \le T \le 800°C, \end{cases} \quad (10)$$

The influence coefficient α_1 (Eq. 7) of temperature on the residual strength of recycled concrete is obtained by fitting.

The influence of recycled coarse aggregate replacement rate on the strength of recycled concrete test block is shown in Figure 14B. The influence coefficient β (Eq. 10) of replacement rate on the residual strength of recycled concrete is obtained by fitting.

After spray cooling at different temperatures, the strength changes of the plain hoop and thread longitudinal reinforcement were also different. The influence of temperature on the tensile strength of longitudinal reinforcement after spraying water at high temperatures is shown in Figure 15A. The influence coefficient α_2 (Eq. 8) of temperature on longitudinal reinforcement after spraying water at high temperature is fitted.

The influence of temperature on the tensile strength of the stirrup after spraying water at high temperature is shown in Figure 15B and the influence coefficient α_3 (Eq. 9) of temperature on the stirrup is obtained by fitting.

Based on the existing formula for calculating the bearing capacity of spiral stirrup members, the influence of temperature and substitution rate on a recycled concrete and the influence of temperature on reinforcement is considered. According to the data obtained from this test, the bearing capacity formula of the spiral stirrup member is corrected by the coefficient, and the corrected bearing capacity formula of the spiral stirrup member is obtained.

The comparison between the calculated and experimental values of the axial compression bearing capacity of the spiral reinforcement recycled concrete column after spraying water at high temperature is shown in Table.5. Among them, the calculated value of bearing capacity is obtained from the modified formula.

The average value of the ratio of calculated value to measured value was .89, and the variance was .017. The bearing capacity calculated by the fitting formula is relatively safe. Therefore, the formula can be used to calculate the bearing capacity of axial compression members experiencing water spraying at high temperatures in practice.

As seen in Table 5, for axial compression members with natural cooling after high temperature, when the temperature exceeds 600°C, the bearing capacity calculated by the formula is significantly higher than the measured value, so the formulas do not apply to this situation.

In summary, Eqs 6–10 applies to the calculation of the axial compression bearing capacity of the spiral-reinforced recycled concrete cylinder after water spraying cooling, which has experienced a maximum temperature of 0°C–800°C and a spiral reinforcement spacing of 30 mm–70 mm, or it can be used for similar axial compression members with natural cooling, which has experienced a maximum temperature not exceeding 600°C.

6 Conclusion

- After high temperatures and spraying water cooling, the concrete protective layer on the exterior of the spiral-reinforced recycled concrete column peeled off firstly, and then the core concrete part continues to play its bearing capacity for some time. Finally, the internal longitudinal reinforcement deformation is too large to squeeze the spiral stirrup, resulting in the loss of bearing capacity. The higher the temperature is, the earlier the first vertical crack occurs.
- The effect of the recycled aggregate replacement ratio on the performance of the specimens was mainly in terms of peak displacement. The peak displacement increases with the growth of the replacement ratio when the temperature exceeds 600°C, but has the opposite trend at temperatures below 200°C.The smaller the spiral stirrup spacing is, the larger the spalling area of the outer concrete is when the specimen is finally destroyed, and the higher the peak load and ductility coefficient are. The specimens with 50 mm and 70 mm spiral bar spacing had better displacement deformation capacity when water spray cooling was used. Comparing the test results at each temperature, it can be seen that a high temperature above 600°C will have a very obvious effect on the mechanical properties of the specimens.
- Compared with natural cooling, cooling by water spraying can reduce the appearance of small cracks on the surface of the specimen, and reduce the peak displacement of the specimen. When the specimen experienced a temperature

of 800°C, water spray cooling can better preserve the remaining load capacity of the specimen, but will reduce the ductility of the specimen.

- Based on the test results, considering the influence of recycled coarse aggregate replacement rate and temperature, the bearing capacity formula of spiral reinforcement members in the specification was modified. The calculated values are in good agreement with the experimental values.

Data availability statement

The raw data supporting the conclusion of this article will be made available by the authors, without undue reservation.

Author contributions

Data curation, XW; investigation, JL; writing original draft, LH and WX; writing-review and editing, ZC.

Funding

This research report was financially supported by the National Natural Science Foundation of China (No. 51578163), Guangxi Science and Technology Base and Talent Special Project (AD21075031), Guangxi Key R&D Project (AB21220012), Central Funding Project for Local Science and Technology Development (ZY21195010), Special fund project for Bagui scholars [(2019) No. 79], Nanning Key R&D Project (20223024).

Acknowledgments

The authors are very grateful for the support of the above project funds.

Conflict of interest

Author LH was employed by the company Guangxi Road and Bridge Group Construction Engineering Co., Ltd.

The remaining authors declare that the research was conducted in the absence of any commercial or financial relationships that could be construed as a potential conflict of interest.

Publisher's note

References

Ajdukiewicz, A. B., and Kliszczewicz, A. T. (2007). Comparative tests of beams and columns made of recycled aggregate concrete and natural aggregate concrete. *J. Adv. Concr. Technol.* 5 (2), 259–273. doi:10.3151/jact.5.259

Algourdin, N., Pliya, P., Beaucour, A. L., Noumowé, A., and di Coste, D. (2022). Effect of fine and coarse recycled aggregates on high-temperature behaviour and residual properties of concrete. *Constr. Build. Mater.* 341, 127847. doi:10.1016/j.conbuildmat.2022.127847

Behera, M., Bhattacharyya, S. K., Minocha, A. K., Deoliya, R., and Maiti, S. (2014). Recycled aggregate from C&D waste & its use in concrete a breakthrough towards sustainability in construction sector: A review. *Constr. Build. Mater.* 68, 501–516. doi:10.1016/j.conbuil

Cao, W., Liu, Q., Zhang, J., Zhang, Y., and Yin, H. (2011). Research on seismic performance of lowrise recycled concrete shear walls. *J. Beijing Univ. Technol.* 37 (03), 409–417.

Cao, W., Zhu, K., Jiang, W., Chen, G., Lin, D., and Peng, S. (2016). Experimental study on stress-strain constitutive relationship of high strength recycled concrete. *J. Nat. Disasters* 25 (02), 167–172. doi:10.13577/j.jnd.2016.0220

Chen, J. (2018). Study on the interfacial bonding property of high strength concrete pipe after simulated fire water cooling. Master's thesis. Nanning (China). Guangxi University.

Chen, Z., Chen, Y., and Yao, K. (2014). Experimental research on mechanical behavior and influence factor of recycled coarse aggregate concretes under triaxial compression. *J. Build. Struct.* 35, 72–81. doi:10.14006/j.jzjgxb.2014.12.010

Chen, Z., Fan, J., Ye, P., and Zhen, W. (2013). Experimental study on mechanical behavior of reinforced recycled aggregate concrete beams. *Build. Struct.* 43 (09), 92–99. doi:10.19701/j.jzjg.2013.09.017

Chen, Z., Jia, H., and Li, S. (2022). Bond behavior of recycled aggregate concrete-filled steel tube after elevated temperatures. *Constr. Build. Mater.* 325, 126683. doi:10.1016/j.conbuildmat.2022.126683

Chen, Z., Ye, P., Xv, J., and Liang, Y. (2015). Mechanical behavior of reinforced recycled aggregate concrete short columns under axial compression after high temperature. *J. Build. Struct.* 36 (06), 117–127. doi:10.14006/j.jzjgxb.2015.06.015

Dai, J., Xu, Z. D., Gai, P. P., and Hu, Z. W. (2021). Optimal design of tuned mass damper inerter with a Maxwell element for mitigating the vortex-induced vibration in bridges. *Mech. Syst. Signal Process.* 148, 107180. doi:10.1016/j.ymssp.2020.107180

De Silva, D., Andreini, M., Bilotta, A., De Rosa, G., La Mendola, S., Nigro, E., et al. (2022). Structural safety assessment of concrete tunnel lining subjected to fire. *Fire Saf. J.* 134, 103697. doi:10.1016/j.firesaf.2022.103697

Dong, H., Wang, P., Cao, W., Zhang, J., and Bian, J. (2013). Experimental study and theoretical analysis on fire resistant performance of recycled concrete tubular structures. *J. Build. Struct.* 34 (08), 65–71. doi:10.14006/j.jzjgxb.2013.08.001

Ercolani, G., Ortega, N. F., Priano, C., and Senas, L. (2017). Physical–mechanical behavior of concretes exposed to high temperatures and different cooling systems. *Struct. Concr.* 18 (3), 487–495. doi:10.1002/suco.201500202

Garcia-Troncoso, N., Li, L., Cheng, Q., Mo, K. H., and Ling, T.-C. (2021). Comparative study on the properties and high temperature resistance of self-compacting concrete with various types of recycled aggregates. *Case Stud. Constr. Mater.* 15, 00678. doi:10.1016/j.cscm.2021.e00678

Ge, T., Xu, Z. D., and Yuan, F. G. (2022). Predictive model of dynamic mechanical properties of VE damper based on acrylic rubber–graphene oxide composites considering aging damage. *J. Aerosp. Eng.* 35 (2), 04021132. doi:10.1061/(asce)as.1943-5525.0001385

Huang, L., Liang, J., Gao, C., and Yan, L. (2021). Flax FRP tube and steel spiral dual-confined recycled aggregate concrete: Experimental and analytical studies. *Constr. Build. Mater.* 300, 124023. doi:10.1016/j.conbuildmat.2021.124023

Kumar, M. V., Siddaramaiah, Y. M., and Raj, S. J. (2022). Shear behaviour of GFRP retrofitted spiral transverse reinforced concrete beams with partially replaced recycled aggregates. *Mater. Today Proc.* 65, 1642–1650. doi:10.1016/j.matpr.2022.04.700

Laneyrie, C., Beaucour, A.-L., Green, M. F., Hebert, R. L., Ledesert, B., and Noumowe, A. (2016). Influence of recycled coarse aggregates on normal and high performance concrete subjected to elevated temperatures. *Constr. Build. Mater.* 111, 368–378. doi:10.1016/j.conbuildmat.2016.02.056

Li, H., Xu, Z., Gomez, D., Gai, P., Wang, F., and Dyke, S. J. (2022). A modified fractional-order derivative zener model for rubber-like devices for structural control. *J. Eng. Mech.* 148 (1), 04021119. doi:10.1061/(asce)em.1943-7889.0002027

Limbachiya, M., Meddah, M. S., and Ouchagour, Y. (2012). Use of recycled concrete aggregate in fly-ash concrete. *Constr. Build. Mater.* 27 (1), 439–449. doi:10.1016/j.conbuildmat.2011.07.023

Liu, B., Chen, L., Zhou, A., Zhen, Y., and Fu, L. (2011). Experimental study on seismic behavior of recycled aggregate concrete beam-column interior-joints. *J. Build. Struct.* 32, 109–115.

Lu, H., Xu, Z. D., Iseley, T., and Matthews, J. C. (2021). Novel data-driven framework for predicting residual strength of corroded pipelines. *J. Pipeline Syst. Eng. Pract.* 12 (4), 04021045. doi:10.1061/(asce)ps.1949-1204.0000587

Lu, Z., and Su, L. (2010). The Chinese research progress on damage mechanism and evaluation on method of concrete structure after fire in China. *J. Build. Struct.* 31 (2), 202–209.

Mohammad, A., Abdulsamee, H., and Amin, A. (2021). Experimental study on compressive strength of recycled aggregate concrete under high temperature. *Struct. Durab. Health Monit.* 15, 335–348. doi:10.32604/sdhm.2021.015988

Muhammad, J. M., Kazmi, S. M. S., Wu, Y. F., Patnaikuni, I., Zhou, Y., and Xing, F. (2020). Stress strain performance of steel spiral confined recycled aggregate concrete. *Cem. Concr. Compos.* 108, 103535. doi:10.1016/j.cemconcomp.2020.103535

Muhammad, J. M., Wu, Y. F., Kazmi, S. M. S., Patnaikuni, I., Zhou, Y., and Xing, F. (2019). Stress-strain behavior of spirally confined recycled aggregate concrete: An approach towards sustainable design. *Resour. Conserv. Recycl.* 146, 127–139. doi:10.1016/j.resconrec.2019.03.043

Ni, S., and Gernay, T. (2020). Predicting residual deformations in a reinforced concrete building structure after a fire event. *Eng. Struct.* 202, 109853. doi:10.1016/j.engstruct.2019.109853

Raza, A., Manalo, A. C., Rafique, U., AlAjarmeh, S., and Khan, Q. Z. (2021). Concentrically loaded recycled aggregate geopolymer concrete columns reinforced with GFRP bars and spirals. *Compos. Struct.* 268, 113968. doi:10.1016/j.compstruct.2021.113968

Shahraki, M., Hua, N., Elhami-Khorasani, N., Tessari, A., and Garlock, M. (2022). Residual compressive strength of concrete after exposure to high temperatures: A review and probabilistic models. *Fire Saf. J.* 2022, 103698. doi:10.1016/j.firesaf.2022.103698

Su, Z., and Chen, Z. (2021). Study on axial compression properties and damage of concrete filled square or circular steel tube columns after being subjected to elevated-temperatures spray cooling. *Fire Sci. Technol.* 40 (12), 1762–1769.

Sun, B., Liu, X., and Xu, Z. D. (2022). A multiscale bridging material parameter and damage inversion algorithm from macroscale to mesoscale based on ant colony optimization. *J. Eng. Mech.* 148 (2), 04021150. doi:10.1061/(asce)em.1943-7889.0002067

Wang, Y., Gong, J., Qu, S., Zhang, B., and Chen, Y. (2022). Mechanical properties of steel reinforced concrete T-shaped column after high temperature. *Structures* 46, 852–867. doi:10.1016/j.istruc.2022.10.117

Wang, Y., Chen, J., Zong, B., and Geng, R. (2011). Mechanical behavior of axially loaded recycled aggregate concrete filled steel tubular stubs and reinforced recycled aggregate concrete stub. *J. Build. Struct.* 32, 170–177. doi:10.14006/j.jzjgxb.2011.12.002

Woo, K. S., Lee, B. S., Kim, Y. S., Lee, S. H., and Kim, K. H. (2018). Structural performance of recycled aggregate concrete confined by spiral reinforcement. *J. Asian Archit. Build. Eng.* 17 (3), 541–548. doi:10.3130/jaabe.17.541

Wu, B. (2003). *The mechanical properties of reinforced concrete structures after fire*. Beijing, China: Science Press, 135–140.

Xiao, J., and Huang, Y. (2006). Residual compressive strength of recycled concrete after high temperature. *J. Build. Mater.* 9 (03), 255–259. doi:10.1016/j.conbuildmat.2016.02.056

Xiao, J., Sun, Y., and Falkner, H. (2006). Seismic performance of frame structures with recycled aggregate concrete. *Eng. Struct.* 28 (1), 1–8. doi:10.1016/j.engstruct.2005.06.019

Xu, Z. D., Yang, Y., and Miao, A. N. (2021). Dynamic analysis and parameter optimization of pipelines with multidimensional vibration isolation and mitigation device. *J. Pipeline Syst. Eng. Pract.* 12 (1), 04020058. doi:10.1061/(asce)ps.1949-1204.0000504

Yu, M., Hu, X., Xu, L., and Cheng, S. (2022). A general unified method for calculating fire resistance of CFST columns considering various types of steel and concrete. *J. Build. Eng.* 59, 105125. doi:10.1016/j.jobe.2022.105125

Zheng, Y., Zhang, Y., and Zhang, P. (2021). Methods for improving the durability of recycled aggregate concrete: A review. *J. Mater. Res. Technol.* 15, 6367–6386. doi:10.1016/j.jmrt.2021.11.085

Zhou, J., Chen, Z. P., Zhou, C. H., and Jin, C. G. (2022). Eccentric compression behavior and bearing capacity calculation of steel-concrete composite square columns confined with spiral bars. *Eng. Mech.* 39. doi:10.6052/j.issn.1000-4750.2021.08.0613